Towards high-resolution multi-sensor gridded ACSPO SST product: Reducing residual cloud contamination

Irina Gladkova*[a,b,c], Alexander Ignatov[a], Mathew Pennybacker[a,c], Yury Kihai[a,c]

[a] STAR, NOAA NCWCP, 5830 University Research Court, College Park, MD, USA 20740
[b] City College Of New York, 160 Convent Ave., New York, NY, USA 10031
[c] Global Science and Technology Inc., College Park, MD, USA 20740

ABSTRACT

Sea Surface Temperature (SST) products at NOAA are produced from multiple polar-orbiting and geostationary sensors using the Advanced Clear-Sky Processor for Ocean (ACSPO) enterprise system. Data of several high-resolution (~1 km) sensors onboard US and EUMETSAT polar-orbiting platforms are processed, including two VIIRSs (onboard NPP and N20), three AVHRR FRAC (onboard Metop-A, -B, and -C), and two MODISs (onboard Terra and Aqua). L1b data of each platform/sensor are processed independently, and two SST products generated: swath (L2P) and 0.02° mapped equal-grid L3U. All L2P and L3U are consistently reported in 10-min granules in a Group for High-Resolution SST (GHRSST) Data Specification Version 2 (GDS2) format, and assimilated in several gridded gap-free L4 analyses, which reconcile data from individual platforms, sensors and overpasses, and fill in cloud obscured regions by optimal interpolation. The L4 feature resolution is degraded, compared to input L2P/3U, with no measure provided of this degradation or identification which grids contain clear-sky observations versus those created by estimation (modeling). There is currently no global SST product based on real observations from all available platforms/sensors, without modeled data. As a result, users either have to rely on L4 products (without knowing what data come from real observations versus those modeled, and how much the satellite data have been smoothed), or deal with huge and ever growing data volumes from multiple L2P/3U data files, and learn how to fuse/aggregate those, themselves. In response to multiple users' requests, NOAA started developing a new multi-sensor, high-resolution, sensor-agnostic gridded L3 SST product, with no modeled data added, which maximally preserves the original sensors' resolution. In creating such collated and super-collated (L3C/S) products, several issues must be addressed, including minimizing the effect of residual cloud leakages, which are always present in the L2P/3U data, on the L3C/S product, while maximally preserving the feature-resolution present in the original satellite imagery. This aspect of data fusion is the focus of this study.

Keywords: Sea Surface Temperature, SST, NOAA, ACSPO, L2P, L3U, L3C, L3S, polar-orbiting, VIIRS, AVHRR, MODIS, high-resolution, collated, super-collated.

1. INTRODUCTION

SST is required in many oceanographic, meteorological and climatological applications, including monitoring of climate variability, operational weather and seasonal forecasting, ocean-atmosphere interaction, military and defense operations, validation and/or forcing of the ocean and atmospheric models, ecosystem assessment, coastal management, tourism, and fisheries. In today's NOAA, and the wider international Group for High-Resolution SST (GHRSST) community, this demand is fulfilled by three flavors of global SST products:

1. L2P (swath): individual granules produced from different overpasses of multiple platforms/sensors. Native-resolution products are large in size, and well suited for analyses of hi-res satellite imagery. They are used as input to various gridded L3 products, and are often fed into L4 analyses and data assimilation (DA). The latter task is becoming more challenging, in recent years, as the number of hi-res (~1-km) sensors and satellites keeps growing. Today, NOAA processes data of seven hi-res sensors, including 2 VIIRSs onboard NPP and N20; 3 AVHRR FRACs onboard Metop-A, -B, and -C; and two MODISs onboard Terra and Aqua. This makes L2P data volumes prohibitive, and an increasing number of L4 producers have switched to the use of reduced volume, high-quality L3U data.
2. L3U (gridded uncollated): individual granules produced from the corresponding L2P granules. Today, NOAA produces a uniform line of 0.02º L3U products from all polar (and geostationary) sensors [1], that are reported as 10-

Ocean Sensing and Monitoring XI, edited by Weilin "Will" Hou, Robert A. Arnone, Proc. of SPIE
Vol. 11014, 110140L · © 2019 SPIE · CCC code: 0277-786X/19/$18 · doi: 10.1117/12.2518462

min granules corresponding to L2P files with 144 files per day. The ACSPO L3U gridding code additionally quality controls L2P data (e.g., removes outliers due to residual cloud). Moreover, it closely preserves the feature resolution of L2P, due to the use of a flexible bilateral algorithm [1]. The NOAA L3U code is also capable of producing higher-resolution L3Us (e.g. 0.01º). Gridded L3Us serve many of the same applications as L2P, and in fact are preferred by many users, due to their smaller size and convenient mapping.

3. L4 (gap-free gridded analyses – e.g., 0.05º STAR geo-polar blended [2]; 0.25º NCEI OISST "Reynolds" SST [3]; 0.10º Canadian Met Centre, CMC [4]; 0.05° Met Office Operational SST and Sea Ice Analysis, OSTIA [5]; 0.01º JPL Multi-Scale Ultra-high resolution, MUR [6] – are produced by assimilation of L2P or L3U data. The L4 processing QC's and modifies input L2P/3U data, and creates new data in missing areas by approximating according to some modeling scheme (e.g. by applying optimal interpolation, or using prior clear-sky observations).

At NOAA, the L2P and L3U data are produced by the enterprise Advanced Clear-Sky Processor for Ocean (ACSPO) system. About 90% of ACSPO users prefer L3U data, which are gridded and much smaller in size (e.g. for VIIRS, 0.4GB/day for L3U vs. 25GB/day for L2P). Despite the fact that all platforms are processed consistently by the same ACSPO system and are reported on the same grid, handling a multitude of 10-min L3U granules from multiple sensors and overpasses still remains a challenge for many users. Moreover, they need to correct for the residual cross-sensor biases, which may be regional, view angle specific, and variable in time. Reducing residual cloud, while taking special care of preserving dynamic oceanic features, is another challenge.

Today, these challenges are most often addressed by creating gap-free L4 analyses, from individual L2P/3U data. The L4 producers bias-correct each input dataset, perform additional QC (to remove "outliers", i.e. data significantly deviating from the "background"), and blend them together. The resulting L4s are gap free, which many users like, but are subject to several limitations. To improve signal-to-noise ratio in the input hi-res L2P/3U data (~1-km/0.02°), L4 SST products are usually reported on a coarser grid (typically, >0.05º; except JPL MUR which is reported at 0.01º). In reality, however, the actual L4 feature resolution is often coarser than their grid size. In clear-sky areas, where L2P/3U data are reported, the oceanic features are smoothed. In L2P/3U data voids (those with no valid SST retrievals), L4 analyses create modeled data (by some flavor of OI, much lower-resolution microwave, or from past history or even climatology), estimating oceanic features. The latter may not be always realistic, especially in areas and during seasons, when cloud cover persists. This is an important limitation, given the current focus of the SST community on hi-res products (as is also manifested in the name of the international SST coordination body, Group for High-Resolution SST, GHRSST).

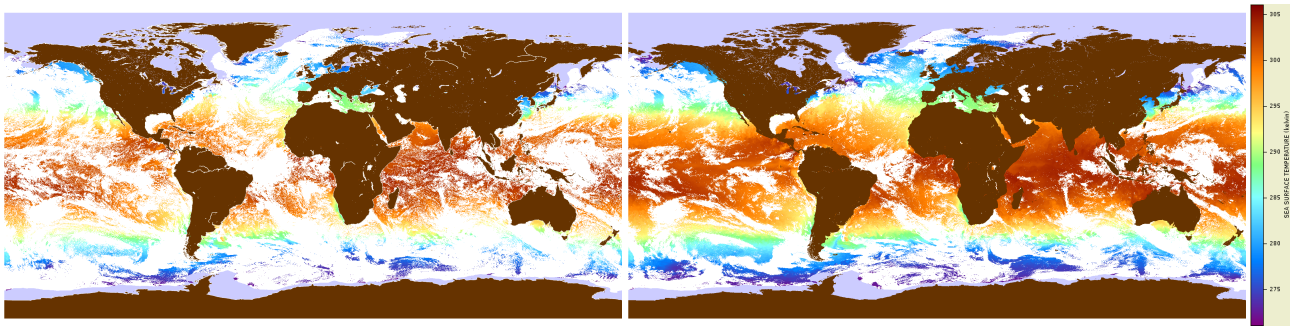

a) b)

Figure 1. SST coverage on 7 Sep 2017: a) NPP VIIRS nighttime; b) Multiple sensors: VIIRS NPP and N20 plus AVHRR MetOp A/B/C.

Notably missing in the current line of NOAA SST products is a group of products with SST values aggregated from all available sensors/platforms/overpasses, and based only on real satellite data, without adding modeled data. Adding observations from multiple overpasses and sensors improves coverage by a factor of ~2 (see example for SNPP VIIRS in Fig. 1). Many users are interested in and requested to add the fused gridded SST product to the line of current L2P & L3U products. To address this users' need, NOAA started developing two fused gridded products: collated L3C (produced from multiple overpasses of the same satellite) and super-collated L3S (produced from multiple overpasses of all available platforms/sensors over the area). The L3C/S products are fundamentally different from L4 as they only contain satellite SST retrievals. Today's users face the dilemma of either dealing with huge (and ever growing) volumes of L2P/3U data and creating their own L3C/S products (without a full understanding of the nature of their remaining errors), or using one of the available L4 products without knowing what data come from real observations and how much

they were smoothed, and what data are extrapolated by OI and/or climatology and what is their quality). Many current SST users opt for the 0.01º L4 MUR product, which indeed appears realistic and preserves hi-res oceanic features in those scenes where high-quality satellite data were available. The MUR quality however degrades in interpolated areas, and where satellite data have suffered cloud leakages. Some users do not fully realize these pitfalls, but many are aware of those but don't have access to suitable L3C/S alternatives.

We believe that a L3C/S product is best produced by our team, which produces the ACSPO L2P/3U products, as we know the strongest sides and shortcomings of the per-swath processing. We have identified several features in the current ACSPO single-sensor, single-pass products, which affect the collation. Namely:

1) Residual cloud leakages in multiple L2P/3U input data. ACSPO employs an accurate and consistent clear-sky mask to all satellites and sensors [7]. Nevertheless, residual cloud leakages is present in the data, which may be platform, sensor, and swath-position specific;
2) Residual inter-satellite and overpass-to-overpass biases. ACSPO employs accurate and consistent SST algorithms to all satellites and sensors [8-9], but residual biases exist, due non-uniform performance of the SST retrieval algorithms in different regions, seasons and across the swath;
3) Residual image "noise" is superimposed on hi-res oceanic features in the original L2P/3U imagery. Much work was devoted in ACSPO to correct for known systematic imagery issues, including striping [10-11] and bow-tie distortions and deletions [12]. However, the effects of random noise in sensor brightness temperatures, and small (often sub-pixel) residual cloud, are amplified by the SST algorithms, and affect the L2P /3U imagery. Different spatial resolution of original L2P data mapped into equal-grid L3U data also affects the image quality.
4) Different overpasses occur at different times, resulting in diurnal changes and evolution of spatial SST features. Special steps should be taken to produce a diurnally resolved product (if feasible), or normalize to a common observation time, and maximally preserve sharpness of spatial patterns in the imagery.

These issues are best accounted for by the L2P/3U data producers, who know them best. This can be done by adopting some post-processing mitigation strategies, at the stage of collation or super-collation. Or, better yet, by fundamental revisions to the L2P retrieval algorithms (e.g., improved clear-sky mask, and SST retrieval algorithms). This study focuses on the first of those four issues, mitigation of residual cloud in the individual L3U imagery being collated. The other two aspect of the collation algorithm are currently being analyzed, and the results will be presented later.

2. METHODOLOGY

2.1 Limitations of simple compositing techniques

An example of two looks at the same scene from NPP and N20 VIIRSs is shown in Fig. 2. The ACSPO mask [7] does a reasonable job on both images, when each is viewed in isolation. Global monitoring of all ACSPO SST L2P/3U products in the NOAA SST Quality Monitor system [13-14] confirms that the ACSPO mask preforms well globally. Nevertheless, there are always remaining small, sub-pixel, and opaque cloud and cloud boundaries, which are very difficult, if at all possible, to detect without using the temporal context. The composite image of average SST values has artifacts due to residual cloud-contaminated pixels, which are prominent in the corresponding scatter plot of the two overpasses plotted against each other. To reduce residual cloud, one may consider removing the colder SST from each pair when the difference between them is significantly large, but this could result in systematic over-screening of the colder sides of the thermal fronts in dynamic regions and does not address the issue with occasional "warm" cloud leakages.

In this study, we present a different approach, described in sections 2.2-2.3, which first constructs a reference using all available overpasses and then compares each individual overpass with this reference. To be applied, the method requires several overpasses, which do not necessarily have to come from hi-res sensors such as VIIRS, MODIS, or AVHRR FRAC. A low-res sensor, if available, such as e.g. AVHRR GAC, can also help. As a quick preview of its outcome, the super-collated image and corresponding scatterplot are also shown in Fig. 2. This technique is particularly useful in challenging areas, where both SST retrievals and clear-sky masking are extremely complex and often suboptimal. Two panels of Fig. 3 show the frequency of night-time overpasses of the Norwegian Sea from two VIIRSs (onboard NPP and N20), and from 6 platforms (2 VIIRSs + 2 AVHRRs + 2 MODISs) with multiple looks will not only lead to a more complete coverage, but also offer potential for improved cloud screening.

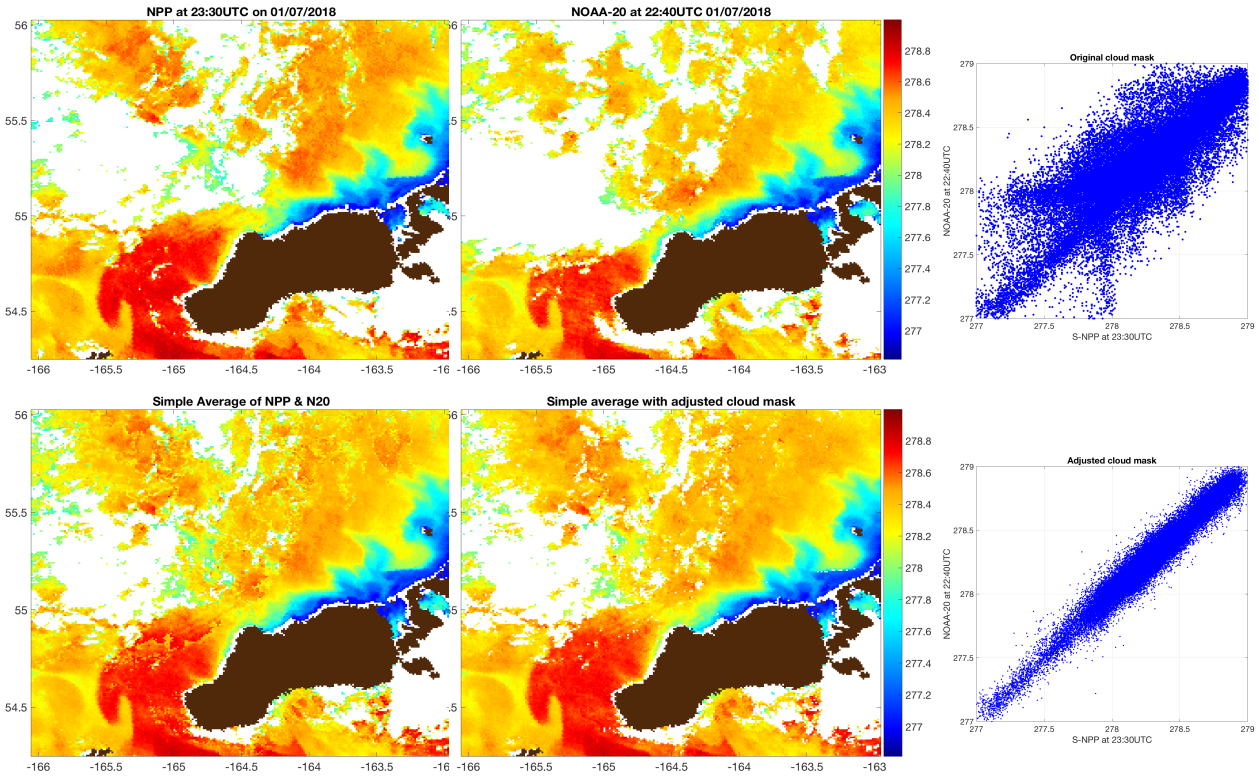

Figure 2. Unimak Island (largest in the Aleutian chain) on 7 January 2018. Top row: two daytime VIIRS overpasses (N20 @22:40UTC and NPP @23:30UTC), along with scatter plot of clear-sky SST values. Bottom row: Simple average of the two overpasses, using (left) original L2P clear-sky mask and (right) adjusted mask obtained using temporal information. The coverage is nearly identical as the multiple overpasses are used to screen-out those less reliable, out of several observations.

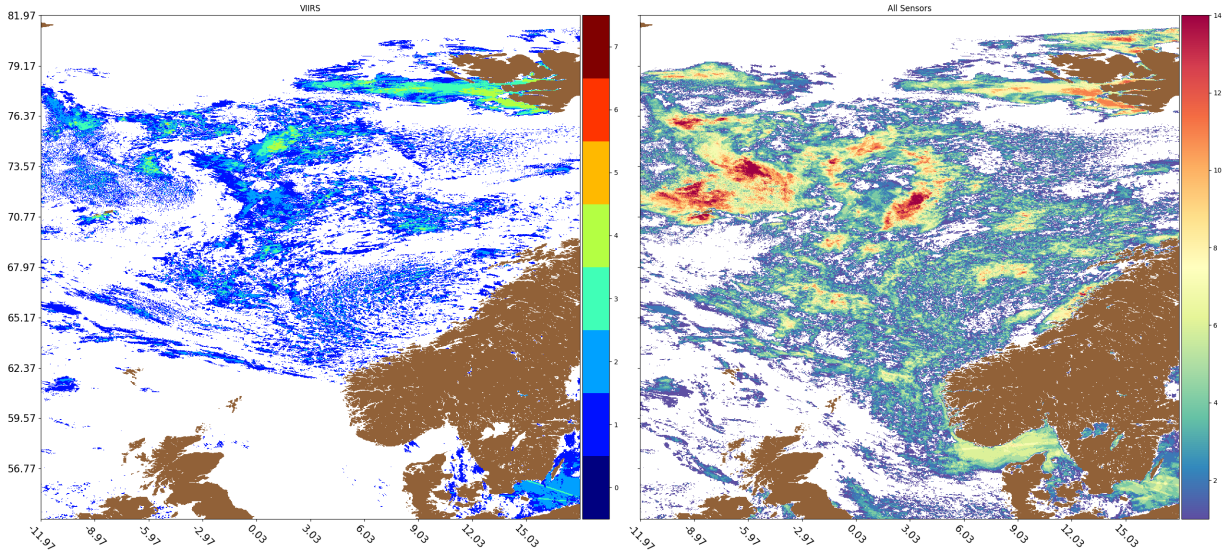

Figure 3. Night-time coverage of the Norwegian Sea: (left) frequency of 2 VIIRSs (NPP+N20) clear-sky counts; (right) frequency of observations form 6 platforms carrying 2 VIIRSs + 2 AVHRRs + 2 MODISs. Additional overpasses, if available, will increase coverage, and further reduce residual cloud leakages (e.g., at the cloud boundaries).

2.2 Approach

This section gives an overview of the approach. The main steps of the algorithm are illustrated in Figs. 4a-c, using 3 VIIRS overpasses on Jan 1, 2019 over Monterey Bay, CA as an example. A good quality high-resolution multi-sensor collation must preserve oceanic features at the original L3U spatial resolution, and exclude features attributed to atmospheric/residual cloud contamination. This objective is achieved through the use of well-established image pyramid techniques of image processing, modified to address the cloud contamination problem present in satellite imagery. Hierarchical representation of the image such as the Gaussian/Laplacian or wavelet image pyramid has been successfully used for decades for image morphing, blending and stitching multiple images into a seamless mosaic [15-16]. Image pyramids can be used to extract image features at multiple scales, and then create a high fidelity composite image from a set of images, parts of which may have different scales. The final fused (super-collated) image (shown in Fig. 7b) has been created with a 3-level pyramid, after additional cloud screening following the steps described below.

Main steps of the algorithm:

1. Compute the simple (per pixel) average $T^{\text{ave}} = \sum T_t$ of all available clear sky SST values T at all available times t (here t represents the UTC start time of a 10-min L2P granule). T^{ave} is a good "first-guess" collated SST, but the image is usually "patchy", due to discontinuities caused by various biases present in individual overpasses and cloud leakages (in this particular example, the bias has been adjusted, to allow focusing on the cloud leakages; cf. Fig 5d).

2. Iteratively compute the image pyramid of a progressively spatially smoother (more blurred) sequence $\tilde{B}^{(1)}, \tilde{B}^{(2)}, \dots, \tilde{B}^{(k)}$ and corresponding hi-resolution features ("details") $D^{(1)}, D^{(2)}, \dots, D^{(k)}$, using windowed averages with increasing spatial window sizes w_k (cf. Fig. 5 with k=3). At each iteration (indexed by k), the computation of $\tilde{B}^{(k)}$ is a windowed average of blurred average from previous step of iteration: $\tilde{B}^{(k)} = \text{Blur}(\tilde{B}^{(k-1)}, w_k)$, with window size w_k ($w_k = 2k + 1$ in Fig. 5). In the straightforward image pyramid construction, the hi-res feature image $D^{(k)}$ would be the difference between blurred images $\tilde{B}^{(k-1)}$ and $\tilde{B}^{(k)}$ from the successive pyramid levels. In the case of retrieved SSTs that could be contaminated by residual cloud, evaluation of $D^{(k)}$s requires additional cleanup. The aggregation process of hi-resolution features from individual sensors into a single (per pyramid level) image with details, $D^{(k)}$, is described in section 2.3.

3. Reconstruct the pyramid approximation as $F^{(k)} = \tilde{B}^{(k)} + \sum_{j=1}^{k} D^{(j)}$. Examples of reconstructed $F^{(k)}$ for a pyramid with k=1,2,3 levels (shown in Fig. 5 d,g,j) show that the hi-resolution oceanic features on the right side of the image are nearly the same for $F^{(1)}$, $F^{(2)}$ and $F^{(3)}$. However, the left side of the image, which was mostly affected by under-screened cloud-contaminated values, is becoming smoother with each consecutive pyramid level. The main objective of this step is to keep the oceanic hi-resolution features and suppress artifacts attributed to image mosaicking. The final $F^{(k)}$ ($F^{(3)}$ in this case; also shown in Fig. 5e), is then used in the next step of the algorithm for additional cloud-screening. (Please note that $F^{(3)}$ is not the final collated SST product, which will be reconstructed using the same procedure, but after adjusting the clear sky domain.)

4. Perform additional cloud screening per overpass, comparing $F^{(k)}$ from the last level of the pyramid in step 3 with SST images T_t for each individual overpass (cf. Fig. 4f-h). This step removes residual cloud leakages, based on multi-sensor information, which was not present at the stage of L2P processing (cf. Fig. 5a-c with 5f-h). This example shows a typical scenario, when cloud boundaries and opaque cloud are very difficult to identify without temporal information. Another approach was considered in [17], using spatial information present at the L2P processing level, but it is much more computationally involved and currently still being tested in ACSPO.

5. Repeat Steps 1-3 using the modified clear-sky domain obtained in the Step 4 for all available overpasses.

Note: The described approach works best if the considered overpasses are close in time (within 1-2 hours). As the time separating the observations used in the collation process increases, the comparison of the images $D^{(k)}$ with oceanic features becomes less reliable at the higher levels of the pyramid (i.e. with small k, corresponding to highest spatial resolution). For the purposes of residual cloud detection, it may be thus practical to take 2-3 consecutive overpasses and proceed as outlined above, obtaining hi-resolution composite(s) of several overpasses that are close in time (c.f. Fig. 7b). In situations with many overpasses spread over several hours, the clear-sky domain modification should be done using a 2-3 hour time window, after which the resultant composites within each time-window should be collated so that the final result captures a middle position of the thermal fronts. This is outside of scope of this paper and will be addressed in future work.

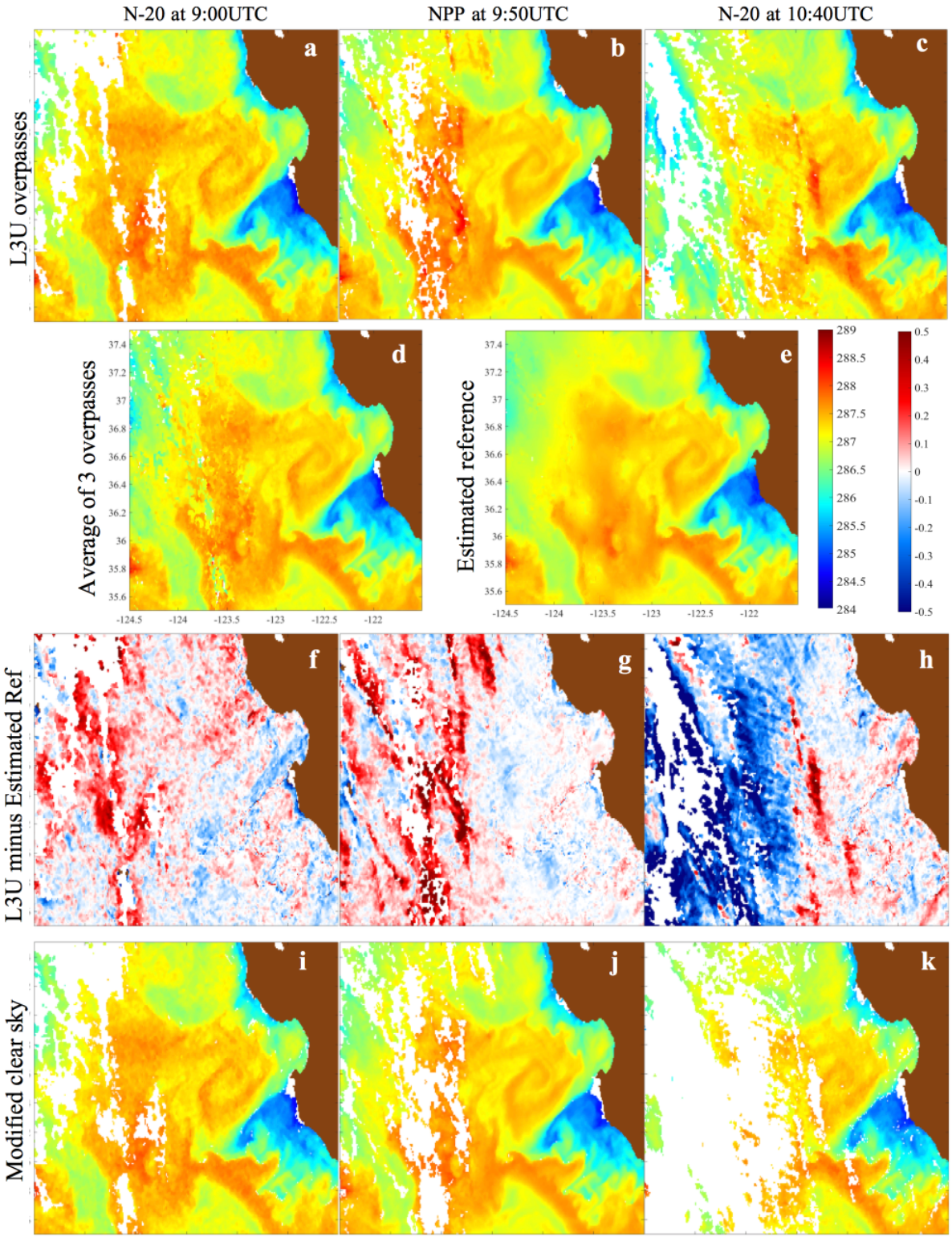

Figure 4. Illustration of steps 1-4 of the algorithm using SST data in Monterey Bay on 1 January 2019. Top row (a-b): original VIIRS L3U SST images at 9:00, 9:50 and 10:40UTC; Second row: (d) simple (per pixel) average; and (e) fused $F^{(3)}$ using the 3-level pyramid approach. Third row (f-h): differences between individual L3Us shown in the top row and fused $F^{(3)}$ shown in (e). Last row (i-k): same as original SST L3U images (shown in the top row) but with modified mask.

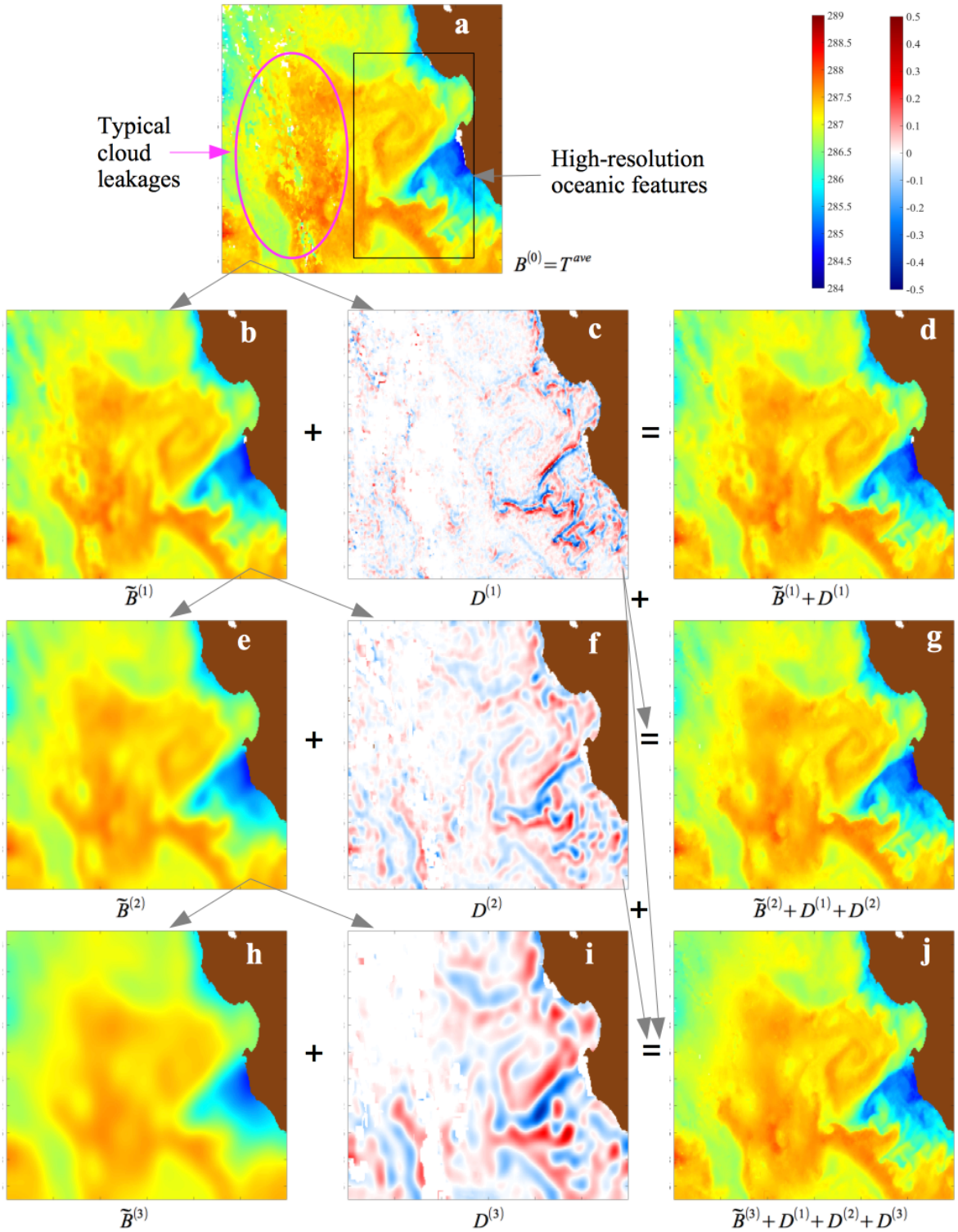

Figure 5. SST data in Monterey Bay on 1 January 2019 (same data as in Fig. 4). Illustration of three levels of image pyramid with blurred images $\tilde{B}^{(k)}$s shown in the first column, feature (details) images $D^{(k)}$s shown in the middle column and resultant $F^{(k)}$s shown in the last column. Note that at each level $D^{(k)}$ is not the difference between successive blurred versions $\tilde{B}^{(k)}$ and $\tilde{B}^{(k-1)}$ as in conventional image pyramid, but the image with oceanic details only, obtained by the process described in Section 2.3 and illustrated in Fig. 6. The fused results are the sum of blurred $\tilde{B}^{(k)}$ and details $\sum_{j=1}^{k} D^{(j)}$ just as in conventional image pyramid.

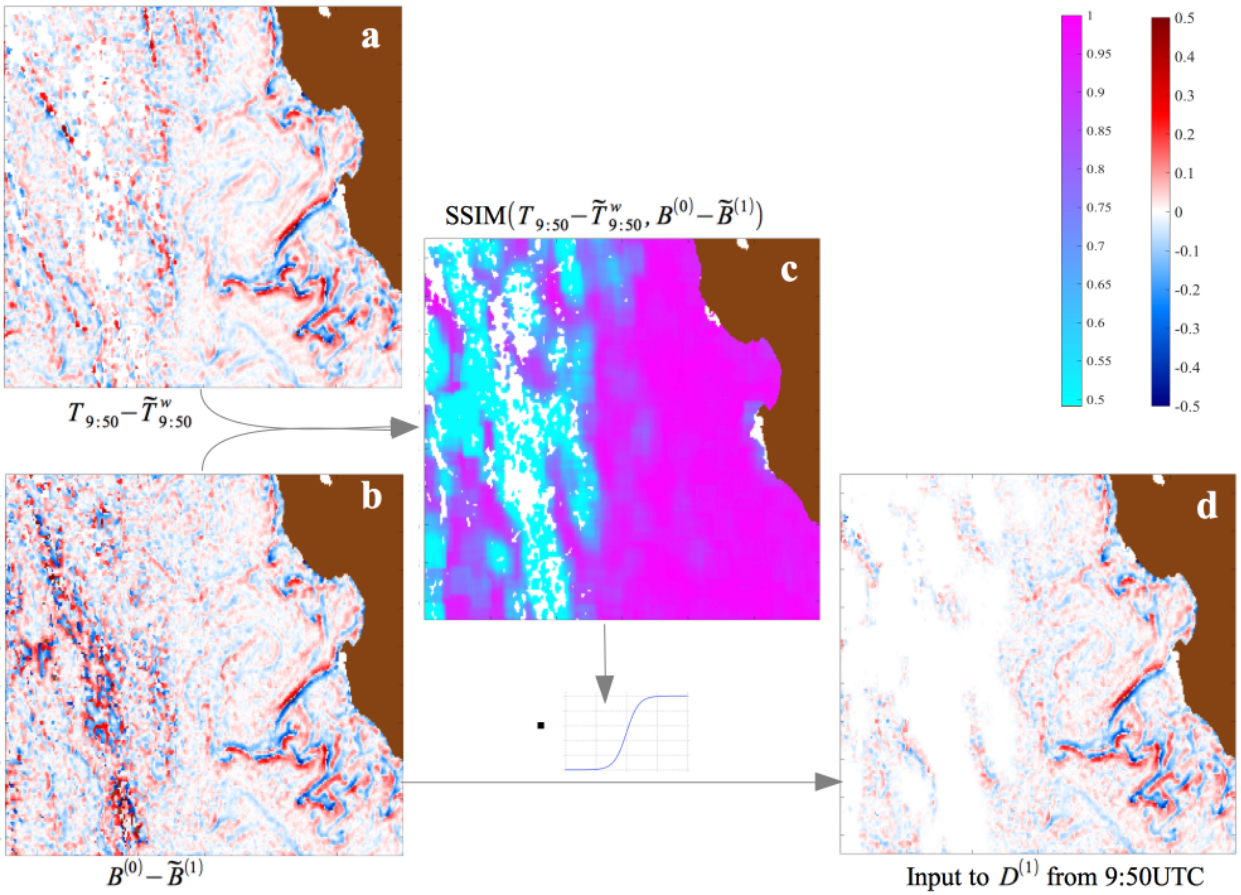

Figure 6. SST data in Monterey Bay on 1 January 2019 (same data as in Figs. 4&5). Example reconstruction of hi-res image $D^{(k)}$ performed at step 2 of the algorithm (k=1 and t = 9:50UTC are used as an example).

2.3 Aggregation of hi-res features

The process of decomposing the image into low-res (blurred) image $\tilde{B}^{(k)}$ and hi-res feature image $D^{(k)}$ is a little more involved than just blurring and subtracting the conventional image pyramid construction. One of the reasons is that distinct overpasses have different cloud mask, which covers different parts of the oceanic features, all of which have to be preserved in the collated product. This reason is intuitively clear and obvious. The other, perhaps a less obvious one, is that although the retrieved SST near the cloud boundary might be within specifications and appear as a noise-like component, the local trends at the cloud boundary might be large enough to produce false features. An example of a difference between the original and blurred version for one individual overpass ($T_{9:50}$ in this case) and the difference between the average $T^{\text{ave}} = \tilde{B}^{(0)}$ and the blurred average $\tilde{B}^{(1)}$ are shown in Fig. 7. In the region where all three overpasses are partially contaminated by cloud, the difference $B^{(0)} - \tilde{B}^{(1)}$ has features that are attributed to artifacts and not to the real oceanic patterns. The hi-resolution features that correspond to artifacts need to be identified and removed so that the resultant image $D^{(k)}$ has only oceanic features, present at least in one of available overpasses. One of the ways to accomplish this is to compare the delta image, containing the details of composite SST, i.e. $\delta_c = B^{(0)} - \tilde{B}^{(1)}$, with delta for each overpass, $\delta_t = T_t - \tilde{T}_t^{w_1}$, and check if the feature is present in at least one of the δ_ts. If it is only present in the delta of the composite product, δ_c (c.f. Fig. 7b), and not in any of the available overpasses, $T_t - \tilde{T}_t^{w_1}$ (c.f. Fig. 7a, which shows only $\delta_{9:50}$ as an example), then it is an artifact of the composition and should not be retained in hi-res feature image $D^{(k)}$ (c.f. Fig. 7d). The window w used in blurring T_t has to be the same as in generation of $\tilde{B}^{(1)}$.

The decision of accepting or rejecting the value $B^{(0)} - \tilde{B}^{(1)}$ at each pixel, can be done by computing Structural SIMilarity (SSIM) Index [18]

$$\mathrm{SSIM}(\delta_t, \delta_c) = \frac{(2\mu_t\mu_c + C_0)(2\sigma_{t,c} + C_1)}{(\mu_t^2 + \mu_c^2 + C_0)(\sigma_t^2 + \sigma_c^2 + C_1)}$$

with 1st and 2nd order statistics μ and σ computed in a window centered at that pixel and having dimension larger than w_1 used in blurring for $\tilde{B}^{(1)}$. We have used a window about twice as large, $2w_1 + 1$, to compute the means μ_t, μ_c, (unbiased) standard deviations σ_t, σ_c of individual overpass δ_t at a time t, and collated δ_c, as well as (unbiased) cross-covariance $\sigma_{t,c}$.The SSIM index [18] has been successfully used in image processing for quality assessment. It combines 3 important factors – similarity of local intensities (represented by mean in the window), contrast (expressed by standard deviation) and structure (represented by cross-covariance). Constants C_0 and C_1 are small values needed for stability in case of small means and standard deviations. The SSIM image is shown in Fig. 7c with $C_0 = C_1 = 0.01$. The decision of keeping or discarding the difference $B^{(0)} - \tilde{B}^{(1)}$ value in each pixel, could be hard- or soft- threshold-based. We have used a sigmoid function centered at 0.8 to suppress features in δ_c with low similarity indices. There might be better options for comparing deltas, which may be explored in the future, if needed. We have preliminarily tested the correlation coefficient along with the SSIM index, and found that the SSIM index is more efficient. The resulting component (QC'ed copy of $D^{(1)}$) obtained using overpass at 9:50UTC is shown in Fig. 7d.

After processing the $D^{(k)}$ with each available overpass, and keeping only the features that are present in that overpass, as described above, the final $D^{(k)}$ contains all features, each of which is present in at least one of the available overpasses.

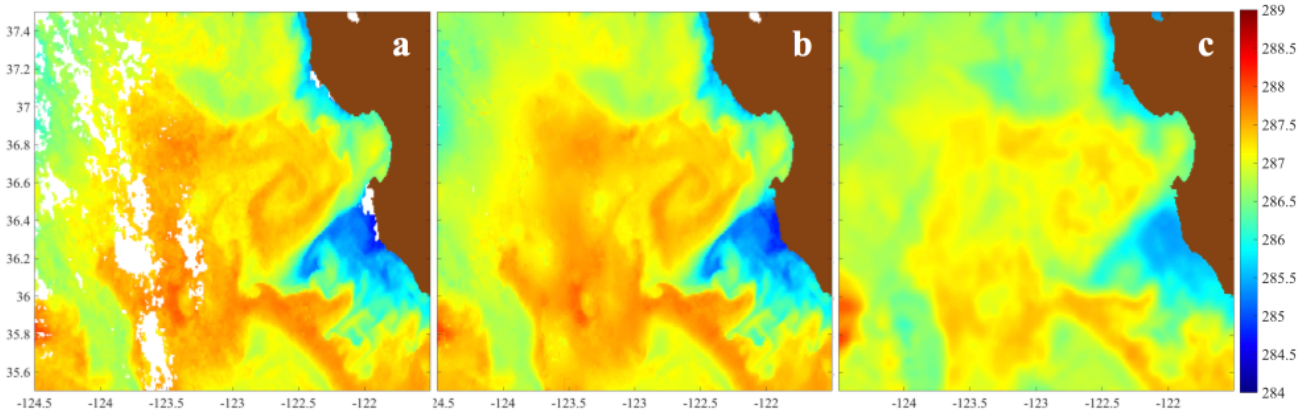

Figure 7. SST data in Monterey Bay on 1 January 2019 (same data as in Fig. 4). a) Simple average using modified mask; b) ACSPO 0.02° super-collated L3S; c) JPL L4 MUR SST product (shown for comparison).

3. DISCUSSION

Evaluation of the performance of the proposed additional cloud screening in ACSPO L3U products, based on multiple looks, has been visual at this point. Although the ACSPO clear-sky mask generally works well and compares favorably with the masks employed in NOAA partners' SST products, it is still subject to residual leakages. Cloud contamination under some challenging conditions (e.g., subpixel, at the cloud boundaries, in the high latitudes, etc.) is very difficult (if at all possible) to detect from a single image (except by a visual inspection of the imagery, and when the temperature range is stretched to around 3-5 K). Below we consider examples representative of two distinct situations, both causing issues for collation.

The first example in Fig. 9 is for the Great Barrier Reef, Australia on 26 March 2019. The scene is covered with many scattered small clouds, which are moving fairly rapidly. This is the case, when aggregation of observations from multiple overpasses will greatly increase the coverage. But, there is a high risk that the resulting product may be subject to artifacts, unless some steps are taken to mitigate the effects of cloud-contaminated observations. Four L3U overpasses used in this example come from two AVHRRs (onboard MetOp-A and -B) and two VIIRSs (onboard NPP and N20). Note that the "mid-morning" Metop AVHRRs (local overpass time ~9:30 am/pm) and "afternoon" JPSS VIIRSs (~1:30 am/pm) are separated by ~3 hours and therefore were processed in groups of 2 at the higher pyramid level (k=1 & 2) and between groups at the lower level (k=3). The resulting super-collated ACSPO L3S is shown in Fig. 8b. The Australian Bureau of Meteorology (BoM) regional multi-sensor super-collated L3S SST product is also shown in Fig. 9c for

comparison. Note that BoM generates multi-sensor SST products for regions of their interest around Australia, including the Great Barrier Reef, using several AVHRR LAC data (from NOAA satellites, such as N18 and N19) and NPP VIIRS. The image in Fig. 9c has noticeable artifacts from cloud contamination. Since the higher-level data producers take L2P/L3U clear-sky flags as the "true" clear-sky observation, their product may have degraded quality. The L4 product (MUR) for the same day is shown in Fig. 9d. Spatial patterns in MUR and ACSPO L3S are generally closer to each other, but in case of numerous small partially cloud-obscured observations, MUR is trying to capture fine-scale features that are attributed to cloud boundary and not to ocean. Note that MUR is using L2P MODIS and NAVO AVHRR GAC as input and these small-scale cloud-related artifacts might be in part related to under-screening by NAVO cloud mask.

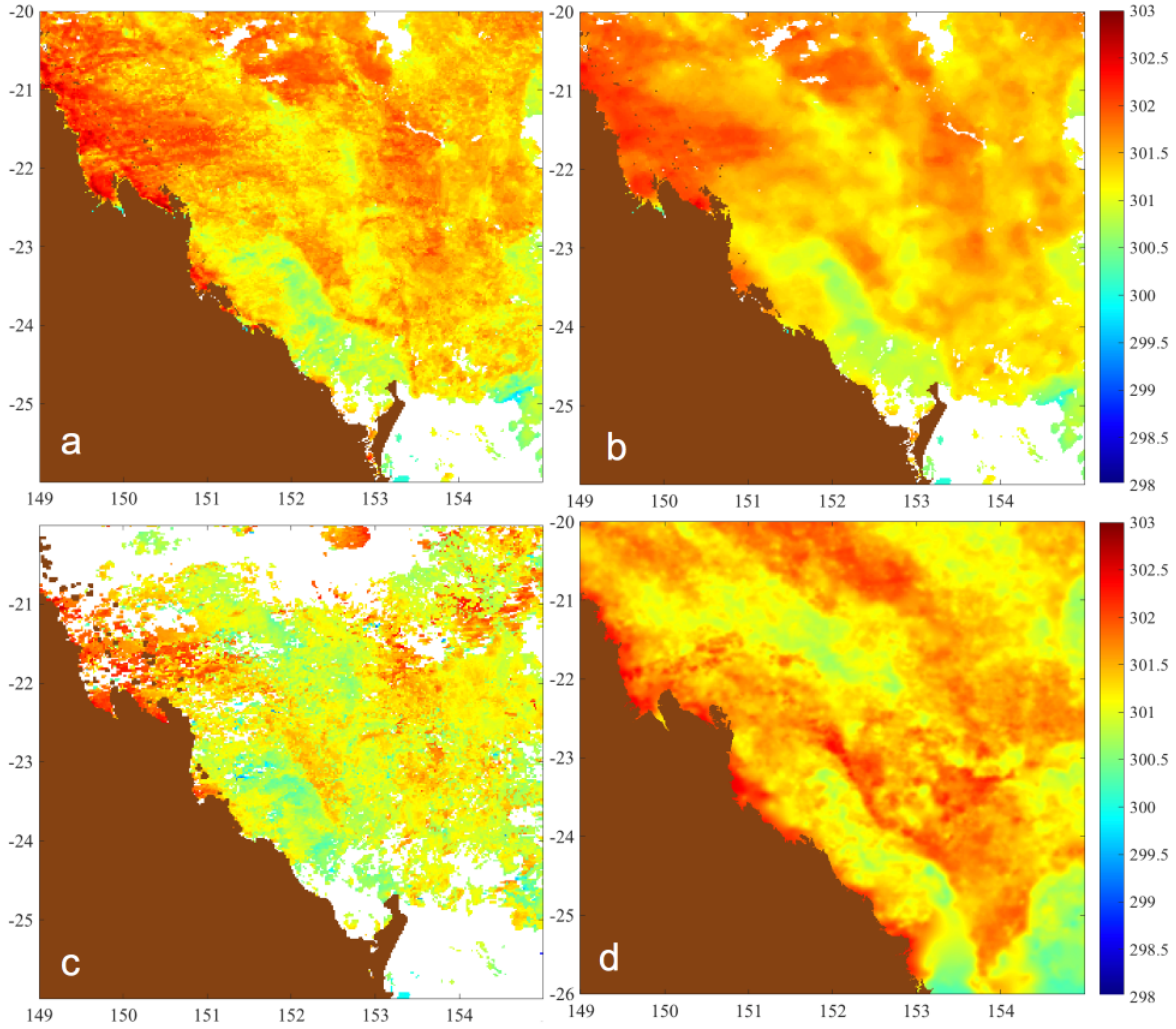

Figure 8. Nighttime SST over the Great Barrier Reef (Australia) on 26 March 2019. a) Average of four ACSPO 0.02° L3U products (from MetOp-B/AVHRR @11:00UTC, MetOp-A/AVHRR @11:30UTC, N20/VIIRS @14:50UTC, and NPP/VIIRS @15:40UTC); b) Prototype super-collated 0.02° L3S using the same four overpasses (generated with 3-level pyramid and cloud screening, as described in this paper); c) Australian Bureau of Meteorology BoM 0.02° L3S product, based on hi-res BoM AVHRR and NOAA ACPSO NPP VIIRS 0.02° L3U products; b) Corresponding 1km JPL MUR L4 SST product. (Note that ACSPO, BoM and MUR SSTs are all shown with their own land-sea masks).

The flip side of the cloud-masking dilemma is over-screening, i.e. falsely labeling clear-sky SST observations as cloud. Once that is done, the downstream users, including L3S and L4 SST producers, do not use these data. One such example is shown in Fig. 9. In this case there are 9 night-time overpasses, almost all of which are clear-sky across the entire region. This is the ideal (and not very frequent) scenario for a collated product. The individual overpasses are not shown here as they look almost identical displayed in the 15K effective range [275 290]K. The super-collated L3S is shown in Fig. 9a and the corresponding L4 MUR in Fig. 9b, for comparison. Despite the availability of multiple clear-sky

overpasses, some hi-resolution oceanic features, present in the L2P data and apparent in L3S, are not present in MUR. The situation when the clear-sky domain is over-screened (as it likely was in the JPL MODIS and NAVO AVHRR L2P data used as input into L4 MUR) is quite typical for dynamic areas, leading to degraded quality of the higher-level products exactly where its hi-resolution potential is needed the most.

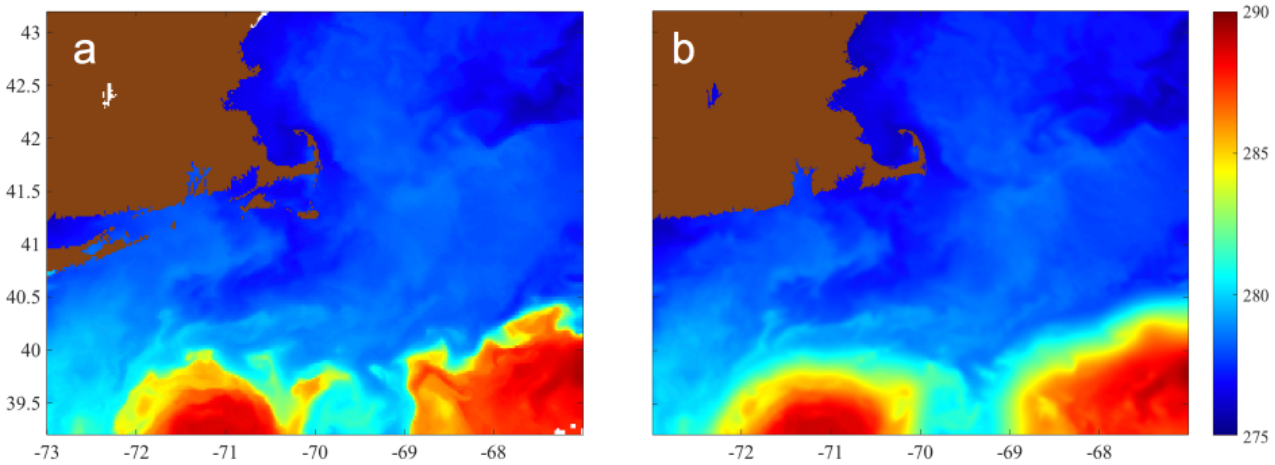

Figure 9. Nighttime SST over the Georges Bank/Nantucket Shoals on 20 March 2019. a) Prototype super-collated 0.02° L3S based on ACSPO L3Us from 9 hi-res overpasses (Metop-A/AVHRR @00:30UTC, MetOp-C/AVHRR @01:00UTC, Metop-B/AVHRR @01:40UTC, MetOp-A/AVHRR @02:10UTC, Terra/MODIS @02:30UTC, NPP/VIIRS @05:20UTC, N20/VIIRS @06:10UTC, Aqua/MODIS @06:40UTC, and NPP/VIIRS @07:00UTC); b) Corresponding 1km JPL MUR L4 SST. (Note that the ACSPO and MUR SST products are shown with their own land-sea masks).

4. CONCLUSION AND FUTURE WORK

We have introduced an algorithm for hi-resolution collation of the SST imagery, which is based on image pyramid construction modified to aggregate imagery with various sensor-specific spatial resolutions, while additionally checking for residual cloud contamination. This step is needed as a part of the ongoing development and implementation of an algorithm for operational generation of hi-res L3S SST product at NOAA. The remaining challenges of the multi-sensor data fusion include sensor-specific residual angular, regional, seasonal, and cross-sensor biases, different spatial resolutions and noise levels in the original L2P data gridded into un-collated L3Us, the varying time of acquisition. This paper is focused on dealing with cloud leakages. The future work will address the issues related to biases of the SST retrievals, specifically the angular, regional and cross-sensor biases. This is a separate, very important for fusion issue, which we need to resolve and present at later time.

5. ACKNOWLEDGEMENTS

This work is supported by the Joint Polar Satellite System (JPSS; Mitch Goldberg, Program Scientist; Arron Layns, JPSS Program Manager; Lihang Zhou, JPSS STAR Program Manager) and NOAA Ocean Remote Sensing (ORS; Paul DiGiacomo and Marilyn Yuen-Murphy, Program Managers) Programs. Thanks go to our SST Colleagues (Boris Petrenko, John Sapper, NOAA, USA; Helen Beggs, Chris Griffin, BoM, Australia) for helpful discussions and feedback. The views, opinions, and findings contained in this paper are those of the authors and should not be construed as an official NOAA or US Government position, policy, or decision.

REFERENCES

[1] Ignatov, A., Gladkova, I., Ding, Y., Shahriar, F., Kihai, Y., Zhou, X., "JPSS VIIRS level 3 uncollated SST Product at NOAA," *J. Appl. Remote Sens.*, **11**(*3*), 032405, doi:10.1117/1.JRS.11.032405 (2017).

[2] Maturi, E., Harris, A., Mittaz, J., Sapper, J, Wick, G., Zhu, X., Dash, P., Koner, P., "A new High-Resolution Sea Surface Temperature Blended Analysis," *BAMS*, **98**(5), 1015-1026, doi:10.1175/BAMS-D-15-00002.1 (2017).

[3] Reynolds, R., Smith, T., Liu, C., Chelton, D., Casey, K., Schlax, M., "Daily high-resolution blended analyses for sea surface temperature", *J. Climate*, **20**, 5473–5496, doi:10.1175/2007JCLI1824.1 (2007).

[4] Brasnett, B., Surcel Colan, D., "Assimilating retrievals of sea surface temperature from VIIRS and AMSR2", *JTech*, **33**, 361-375, doi:10.1175/JTECH-D-15-0093.1 (2016).

[5] Donlon, C.J., Martin, M., Stark, J., Roberts-Jones, J., Fiedler, E., Wimmer, W. "The Operational sea surface temperature and sea ice analysis (OSTIA) system", *Remote Sens. Environ.*, **116**, 140-158, doi:10.1016/j.rse.2010.10.017 (2012).

[6] Chin, T., Vazquez, J., Armstrong, E., "A multi-scale high-resolution analysis of global sea surface temperature", *Remote Sens. Environ.*, **200**, 154-169, doi:10.1016/j.rse.2017.07.029 (2017).

[7] Petrenko, B., Ignatov, A., Kihai, Y., Heidinger, A., "Clear-sky mask for the Advanced Clear-Sky Processor for Oceans," *JTECH*, **27**(*10*), 1609-1623, doi:10.1175/2010JTECHA1413.1 (2010).

[8] Petrenko, B., Ignatov, A., Kihai, Y., Stroup, J., Dash, P., "Evaluation and selection of SST regression algorithms for JPSS VIIRS", *JGR*, **119**, 4580–4599, doi: 10.1002/2013JD020637 (2014).

[9] Petrenko, B., Ignatov, A., Kihai, Y., Dash, P., "Sensor-Specific Error Statistics for SST in the Advanced Clear-Sky Processor for Ocean", *JTECH*, **27**, 345–359, doi: 10.1175/JTECH-D-15-0166.1 (2016).

[10] Bouali, M., Ignatov, A., "Adaptive reduction of striping for improved sea surface temperature imagery from Suomi National Polar-Orbiting Partnership (S-NPP) Visible Infrared Imaging Radiometer Suite (VIIRS)", *JTECH*, **31**(*1*), 150–163, doi: 10.1175/JTECH-D-13-00035.1 (2014).

[11] Mikelsons, K., Ignatov, A., Bouali, M., Kihai, Y., "A fast and robust implementation of the adaptive destriping algorithm for SNPP VIIRS and Terra/Aqua MODIS SST", Ocean Sensing and Monitoring VII, *Proc. SPIE*, **9459**, 94590R-1, doi: 10.1117/12.2177036 (2015).

[12] Gladkova, I., Ignatov, A., Shahriar, F., Kihai, Y., Hillger, D., Petrenko, B., "Improved VIIRS and MODIS SST Imagery," *Remote Sens.*, **8**(*1*), 79, doi: 10.3390/rs8010079 (2016).

[13] SST Quality Monitor (SQUAM) https://www.star.nesdis.noaa.gov/sod/sst/squam/

[14] Dash, P., Ignatov, A., Kihai, Y., Sapper, J., "The SST Quality Monitor (SQUAM)," *JTECH*, **27**(*11*), 1899-1917, doi:10.1175/2010JTECHO756.1 (2010).

[15] Adelson, E., Anderson, C., Bergen, J., Burt, P., Ogden, J., "Pyramid methods in image processing," *RCA Engineer*, **29**(*6*), 33-41 (1984).

[16] Burt, P., Adelson, E., "The Laplacian Pyramid as a Compact Image Code," *IEEE Trans. Comm*. **9**(*4*): 532-540, doi:10.1109/TCOM.1983.1095851 (1983).

[17] Gladkova, I., Kihai, Y., Ignatov, A., Shahriar, F., Petrenko, B., "SST Pattern Test in ACSPO Clear-Sky Mask for VIIRS," *Remote Sens. Environ.*, **160**, 87-98, doi:10.1016/j.rse.2015.01.003 (2015).

[18] Wang, Z., Bovik, A.C., Sheikh, H.R., Simoncelli, E.P., Image Quality Assessment: From Error Visibility to Structural Similarity, *IEEE Trans. Image Proc.*, **13**(*4*), 600-6012, doi: 10.1109/TIP.2003.819861 (2004).